

ACKNOWLEDGMENT

This work was supported by the U.S. Department of Energy Division of Inertial Fusion under agreement No. DE-FC03-85DP40200 and by the Laser Fusion Feasibility Project at the Laboratory for Laser Energetics, which has the following sponsors: Empire State Electric Energy Research Corporation, New York State Energy Research and Development Authority, Ontario Hydro, and the University of Rochester.

REFERENCES

1. S. Skupsky and T. Kessler, *Opt. Commun.* **70**, 123 (1989).
2. R. H. Lehmberg, A. J. Schmitt, and S. E. Bodner, *J. Appl. Phys.* **62**, 2680 (1987).
3. C. Strangio and A. Caruso, *Laser and Particle Beams* **8**, 135 (1990).
4. X. Deng *et al.*, *Appl. Opt.* **25**, 377 (1986).
5. Y. Kato *et al.*, *Phys. Rev. Lett.* **53**, 1057 (1984).
6. LLE Review **33**, 1 (1987).
7. T. Kessler, W. Castle, N. Sampat, S. Skupsky, D. Smith, and S. Swales, in *Proceedings of Conference on Lasers and Electro-Optics*, Optical Society of America, Anaheim, CA, 25–29 April 1988.
8. S. Skupsky, R. W. Short, T. Kessler, R. S. Craxton, S. Letzring, and J. M. Soures, *J. Appl. Phys.* **66**, 3456 (1989).
9. LLE Review **37**, 40 (1988).
10. T. Gunderman, J.-C. Lee, T. J. Kessler, S. D. Jacobs, D. J. Smith, and S. Skupsky, in *Proceedings of Conference on Lasers and Electro-Optics*, Optical Society of America, Anaheim, CA, 21–25 May 1990.
11. “Laser Speckle and Related Phenomena,” in *Topics in Applied Physics*, edited by J. C. Dainty (Springer-Verlag, Berlin, Heidelberg, New York, 1975), Vol. 9, Chap. 2.
12. S. D. Jacobs, K. A. Cerqua, K. L. Marshall, A. Schmid, M. J. Guardalben, and K. J. Skerrett, *J. Opt. Soc. Am. B*, **5**, 1962 (1988).
13. S. Papernov, K. Marshall, M. Guardalben, A. Schmid, and S. D. Jacobs, *Liq. Cryst.* **9**, 71 (1991).

1.B Hydrodynamic Simulation of Non-LTE Atomic Physics of High-Density Implosions of Argon-Filled, Polymer-Shell Targets

Implosions of argon-filled, plastic-shell targets provide a source for studying the x-ray emission from matter at high temperatures and densities.¹ X-ray line emission itself can be used to diagnose the core conditions in inertial confinement fusion (ICF) targets. Comparison of the core conditions with hydrodynamic simulations can then provide information on target perfor-

mance, especially on the effect of laser-illumination nonuniformity. Two series of experiments were carried out at the Laboratory for Laser Energetics (LLE), in which Ar-filled plastic microballoons were imploded using the 24-beam UV OMEGA laser system.^{1,2} The two series had different target radii, fill pressures, and laser conditions. The x-ray emission, measured with both time-integrated and time-resolved spectrographs, showed both emission line broadening and absorption-line features. Analysis of the x-ray line emission from the first series of experiments indicated that core electron densities reached 10^{25} cm^{-3} with peak electron temperatures about 1 keV¹ and that a density and temperature gradient existed in the core during the time of emission.²

In the following sections we describe the results of the experiments and the corresponding simulations with the hydrodynamic code *LILAC*. In particular, we show from the results of the simulations that the density-broadened lines are emitted during shock convergence to the target center and that the absorption features occur as the shock travels outward after reflection at the target center. This implies that the line emission and the absorption features from the argon core do not measure the peak densities reached at stagnation. Simulations predict a density and temperature gradient in the absorbing region with magnitudes similar to those measured in the experiment. Also, the timing of the occurrence of the emission and absorption spectral features in the simulations agrees well with experimental observations.

First Series of Experiments

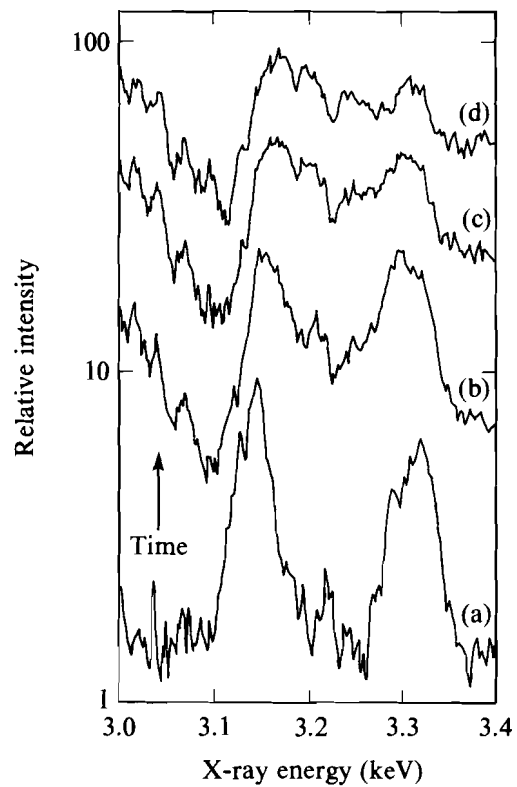
In the first series of experiments,¹ 420- μm diameter, Ar-filled plastic microballoons with 6- μm shell thickness were imploded using the 24-beam UV ($\lambda = 0.351 \mu\text{m}$) OMEGA laser system. The 680-ps (FWHM) Gaussian pulses provided 1700 J of incident energy. The targets were filled with 10 atm of Ar and were coated with a 0.05- μm layer of Al as a retention barrier for Ar and to prevent the shinerthrough of the laser light early in the pulse. It is assumed that argon gas remained diffused into the plastic after the filling process. Improved illumination uniformity was achieved through the use of distributed phase plates (DPP's). The diagnostics included time-resolved x-ray line spectroscopy using SPEAXS³ and time-integrated x-ray spectroscopy. The time-resolved line-emission spectra, analyzed in Ref. 1, showed that the He-like satellites ($2l2l'-1s2l$) of the Lyman-alpha (L_{α}) transition of Ar^{+17} ($1s-2p$) and the resonant transition merged into a single emission feature because of broadening. Electron densities were obtained by comparing the measured line shapes with Stark-broadened line profiles computed from a multielectron line-profile code.⁴ The density and temperature results from that analysis for shot 15772 are shown in Table 45.I.

More recently, the absorption line profiles for the $n = 1$ to $n = 2$ inner-shell transitions present in the time-resolved spectrum for shot 15772 have also been analyzed.² Line-outs from this spectrum at different times during the appearance of the absorption feature are shown in Fig. 45.8. The absorption lines for B-, Be-, and Li-like Ar are seen on the low-energy side of the He_{α} line. The absorption array appears about 50 ps after the broadened

Table 45.I: Density and temperature results from the analysis of data in Ref. (1). Time is measured with respect to the peak of the laser pulse ($1 \times 10^{24} \text{ cm}^{-3} \approx 4 \text{ g/cm}^{-3}$).

Time Interval (ps)	Electron Density (10^{24} cm^{-3})	Temperature (eV)
312–375	3–6	600–900
348–405	5–7	600–800
375–427	6–8	500–800

TC2913



TC2902

Fig. 45.8 Time-resolved x-ray spectrum for shot 15772 in the first series of experiments. These lineouts have been shifted vertically by arbitrary amounts for clarity.

L_α and He-like satellites and is still observed well after the emission lines have merged into the continuum. Stark-broadened absorption profiles, computed from an extended version of the multielectron line-profile code in Ref. 4,⁵ were compared to the experimental spectrum for each absorption line using a simple model of attenuation through a uniform absorption layer,

$$I(\nu) = I_0(\nu) \exp(-\tau_\nu),$$

$$\tau_\nu = \frac{\pi e^2}{mc} f \phi(\nu) N_g l,$$

where $I_0(\nu)$ is the incident intensity, $I(\nu)$ is the attenuated intensity, τ_ν is the optical thickness at frequency ν , f is the average oscillator strength of the 1s–2p absorption transitions of each absorbing ion, $\phi(\nu)$ is the absorption profile, N_g is the absorbing ion density, and l is the path length. The comparison with the experimental spectrum is done in the log (intensity) versus energy plot, and the continuum level is estimated over a broad energy range.

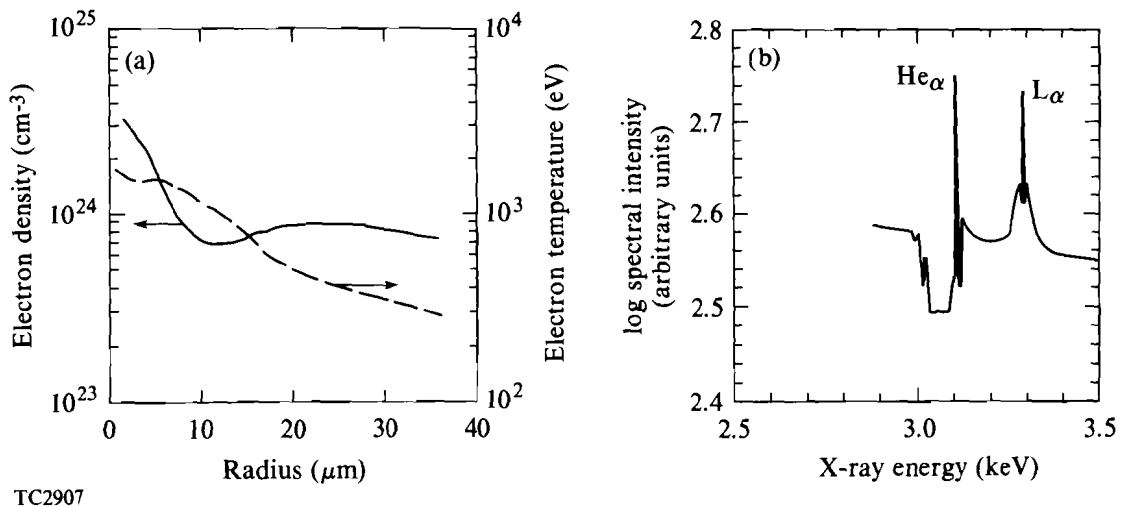
The analysis was carried out for the two line-outs (c) and (d) in Fig. 45.8. For line-out (c), the best fit to the overall absorption features was obtained by using electron densities $n_e = 2 \times 10^{24} \text{ cm}^{-3}$ for the B-like Ar and $n_e = 1 \times 10^{25} \text{ cm}^{-3}$ for the Be- and Li-like Ar. Changing the electron temperature from 200 eV to 600 eV did not produce significant differences in the shape of the line profile. The analysis of the absorption feature of line-out (d) yielded similar results: n_e in the range $1 \times 10^{24} \text{ cm}^{-3}$ to $2 \times 10^{24} \text{ cm}^{-3}$ fits the B-like Ar transitions, and $n_e = 5 \times 10^{24} \text{ cm}^{-3}$ fits the Be- and Li-like Ar transitions.

The results of the analysis of the time-resolved spectrum for shot 15772 indicate that densities larger than $5 \times 10^{24} \text{ cm}^{-3}$ have been achieved in the compressed argon. The fact that two different sets of values for the electron density and temperature were needed to fit the absorption features produced by different ionization states can be attributed to the presence of spatial density and temperature gradients in the argon core. These conclusions will be supported by the results of the simulations.

The simulation of shot 15772 was carried out with the one-dimensional (1-D) hydrodynamic code *LILAC*, a Lagrangian code that includes flux-limited diffusion thermal-electron heat transport, multigroup flux-limited diffusion radiation transport, either local-thermal-equilibrium (LTE) or non-LTE (average-ion model) atomic physics, SESAME equation of state, and ray tracing with a realistic laser-beam profile. The emission spectrum is generated by a postprocessor that includes a detailed-configuration non-LTE model.⁶ This postprocessor does not include the presence of satellites and uses *ad hoc* absorption linewidths (trapezoidal line shape with 21-eV FWHM, separated by 22.4 eV). The energies are roughly estimated from the results of an atomic-structure code that provides the spectral distribution and strengths of the individual transitions. A flux-limiter value of 0.06 (sharp cut-

off method) was used in the electron heat transport. This value, used in all the implosion simulations carried out at LLE, provides good agreement with both the measured absorption fraction and the shell-implosion velocity. In these simulations, it was assumed that the density of the argon dissolved in the plastic shell was equal to that in the fill.

The observed occurrence of broad line emission followed by the appearance of absorption lines can be explained by looking at the shock dynamics in the argon fill during the implosion. In gas-filled target implosions, the gas is heated by a shock wave produced by the inward motion of the shell. The shock wave converges to the target center where it is reflected back toward the imploding shell. Each passage of the shock results in higher densities and temperatures. Conditions in the Ar and the simulated spectrum when the shock is reflected at the center of the target are shown in Fig. 45.9. At the center of the target, the shock-heated Ar has reached electron temperatures in excess of 1 keV and electron densities of $3 \times 10^{24} \text{ cm}^{-3}$. The outer part of the core is colder and less dense than the central part. The simulated spectrum shows both the early absorption features and the Ar L_{α} emission, which is composed of a strong narrow part emitted by the argon present in the shell and heated by the laser, and a weaker broad base emitted by the dense argon in the core. The narrow part of the line is not observed experimentally at this time (see Fig. 45.8) but can be seen earlier, before the onset of emission from the core. This may be because the density of the argon diffused in the plastic may be much lower than expected. The width of the L_{α} line in Fig. 45.9 cannot be directly compared with that in the experiment because the



TC2907

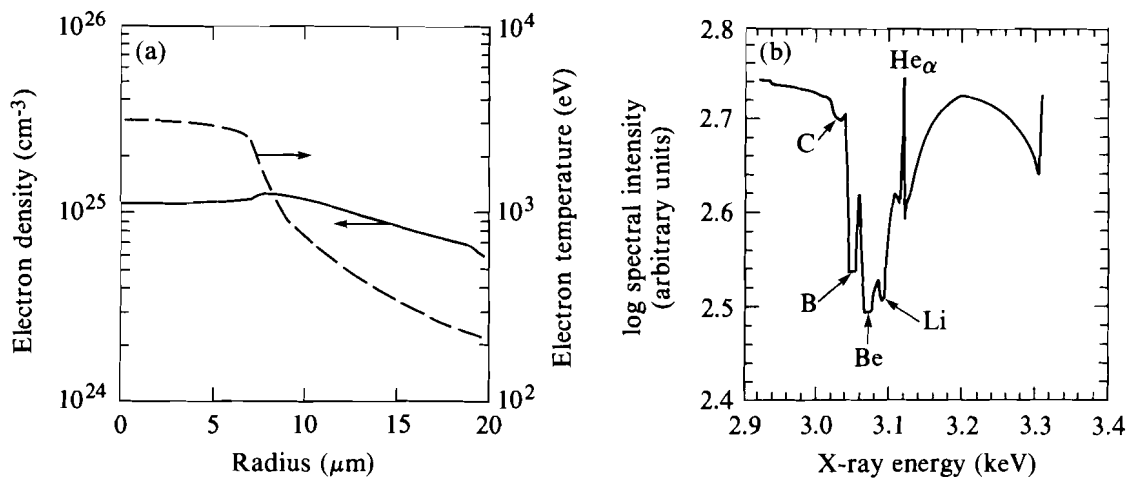
Fig. 45.9

(a) Electron density (solid line) and temperature profiles (dashed line), and (b) simulated spectrum, showing the broadened He α line for shot 15772. The time is 380 ps, with respect to the peak of the pulse, when the shock is reflected at the target center.

postprocessor does not include satellite emission. The conditions in the emitting region of the Ar compare reasonably well with the measured electron densities and temperatures listed in Table 45.I. As in the experiment, the computed electron density increases with time while the temperature drops slightly because of radiative cooling. The observed temperatures are lower than the computed values probably because the experimental implosion is not perfectly one-dimensional.

The conditions in the Ar core later in time are shown in Fig. 45.10(a), when the shock, after reflection at the target center, is almost halfway back across the core on its way to the plastic shell (at the right edge of the graph). At this time, the electron temperature has dropped to 1 keV, but the electron density has reached $3 \times 10^{25} \text{ cm}^{-3}$ behind the shock. Under these extreme conditions the central region of the Ar core will emit mostly a continuum spectrum. As this emission travels outward, it passes through the cooler and less dense outer region of the core, where it is absorbed by $n = 1$ to $n = 2$ inner-shell transitions. Three absorption lines, Li-, B-, and Be-like, are observed in the spectrum computed by the postprocessor and shown in Fig. 45.10(b). These are the same absorption lines that are observed experimentally in trace (b) and (c) of Fig. 45.8. Since the line-absorption model in the postprocessor does not include accurate, realistic line profiles that are density dependent, the comparison between the experiment and simulation set of absorption lines should not be regarded as quantitative.

Fig. 45.10
 (a) Electron density (solid line) and temperature profiles (dashed line), and (b) simulated spectrum, showing the absorption lines for shot 15772. The time is 450 ps, with respect to the peak of the pulse, when the shock has reflected about halfway to the plastic shell. The absorption lines range from Li-like to C-like.



TC2906

Although detailed comparison of the line shapes is not available at this time, we can still compare the simulation results with the experimental results in terms of spatial gradients and ionization-state populations. The density and temperature profiles in Fig. 45.10(a) do show both a density and a temperature gradient in the absorbing region, as was suggested by the

analysis of the experimental absorption-line shapes. The ionic population fractions in the Ar core obtained from the postprocessor at the same time as for Fig. 45.10 are shown in Fig. 45.11 as a function of the radius. The Li-like population is relatively constant throughout the core, whereas the B-like population has a minimum where the shock is located. Thus, we would expect that the absorption by the Li-like transition would be dominated by the higher electron density near the core center (5 to $10 \times 10^{24} \text{ cm}^{-3}$), while the absorption by the B-like transition should be more representative of the lower electron densities near the outer region of the core (2 to $3 \times 10^{24} \text{ cm}^{-3}$). This is in quantitative agreement with the results of the analysis of the observed spectra, which indicate electron densities of $5 \times 10^{24} \text{ cm}^{-3}$ for the Li- and Be-like transitions, and 1 to $2 \times 10^{24} \text{ cm}^{-3}$ for the B-like transitions. There is also a good agreement as to the time at which the absorption features are observed: the trace for spectrum (b) of Fig. 45.8 was averaged over the time interval 400 to 455 ps after the peak of the pulse; the simulation conditions shown in Figs. 45.10 and 45.11 were taken at time 450 ps. The conditions for observing the absorption lines persist until the shock nears the edge of the Ar core. At this time, the core is a very dense sphere of hot Ar at electron densities near or exceeding $1 \times 10^{25} \text{ cm}^{-3}$ and at temperatures slightly lower than 1 keV, and no structure, except for the emission from the argon in the shell, should be observed in the spectrum.

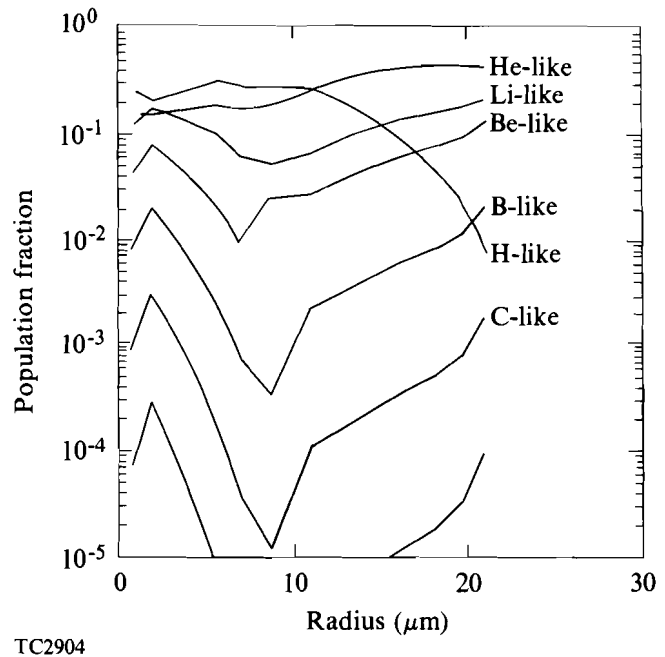


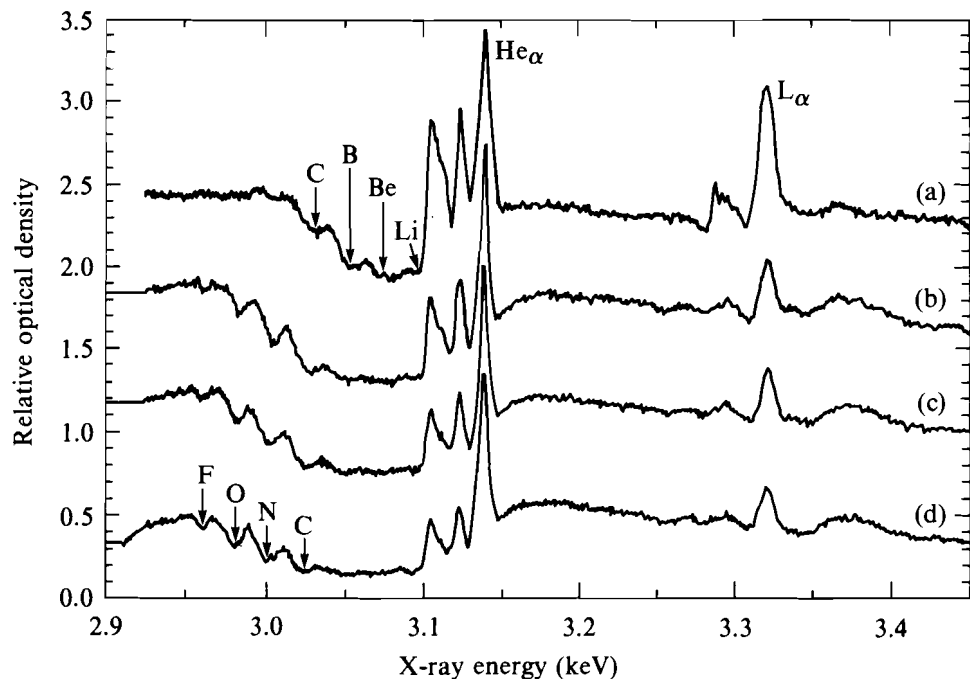
Fig. 45.11
Population fractions for the $n = 1$ to $n = 2$ inner-shell transitions for the conditions in Fig. 45.10.

The distribution of the population fractions shown in Fig. 45.11 as a function of the radius can be explained as follows. When the shock is being reflected at the center of the core, the Ar core consists mainly of an electron-temperature gradient ranging from 200 eV near the outer edge to 1000 eV near the center of the core and of a slowly rising electron density above $1 \times 10^{24} \text{ cm}^{-3}$. (This condition occurs at a slightly later time than that of Fig. 45.9.) The increase in temperature across the core results in a slowly increasing population fraction for the H-like ionization state combined with decreasing populations for the lower ionization states. As the reflected shock traverses this plasma, the increase in electron temperature leads to an increase in ionization. Behind the shock, the electron temperature decreases slightly because of radiation losses, causing the ionization to decrease. The increase in ionization by the shock explains the drop in the population fraction of the lower ionization states.

Second Series of Experiments

In the second series of experiments, Ar-filled microballoons with diameters of 250 μm and plastic thicknesses of 6, 8, 10, and 12 μm were imploded with 600-ps (FWHM), 1200-J Gaussian pulses. The targets were filled with 20 atm of Ar and coated with 0.05 μm of Al. The 24 OMEGA beams included smoothing by spectral dispersion (SSD)⁷ at a frequency of 8.45 GHz with a bandwidth $\Delta\lambda/\lambda = 2.7 \times 10^{-4}$. Only the time-integrated spectra, shown in Fig. 45.12, were available for analysis because the time-resolved spectra were too weak to be analyzed in the same manner as the

Fig. 45.12
Time-integrated x-ray spectra for targets with increasing wall thickness in the second series of experiments. The wall thicknesses are (a) 6 μm , (b) 8 μm , (c) 10 μm , and (d) 12 μm .

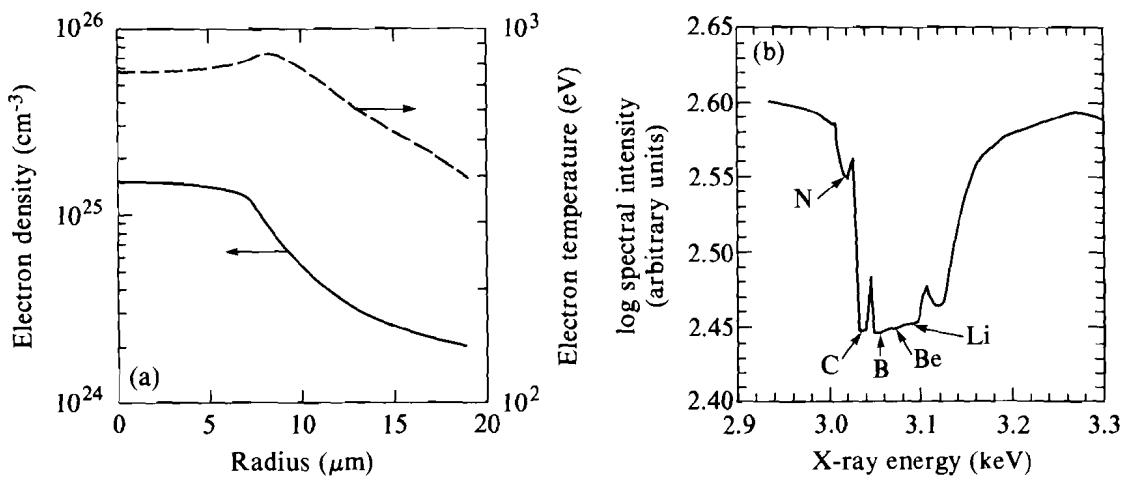


time-resolved spectrum for shot 15772. No detailed analysis was carried out for the absorption features visible on the low-energy side of the He_α resonance line. The spectra show that the lowest ionization state observed in each spectrum decreases as the plastic thickness increases: from C-like for the 6- μm -thick target to F-like for the 12- μm -thick target. This observation implies that the absorbing region of the Ar core is colder in the thick-walled target implosions than in the thin-walled target implosions. Unlike the first series of experiments, the broad emission feature consisting of the density-broadened He-like satellites and the L_α resonance line was not observed. Preliminary results from simulations indicate that the emission level of the Stark-broadened Ar L_α in the second series of experiments should be lower than that in the first series. Thus the time-integrated L_α emission is probably dominated by the narrow emission from the Ar dissolved into the plastic and directly heated by the laser in the corona.

In this series of experiments, simulations were carried out for only two plastic thicknesses: 6 μm and 12 μm . The electron temperatures and densities from the simulation for the 6- μm case are similar to the results of the simulations of shot 15772. (The reduction in target diameter, and hence in the mass, was compensated for by a reduction in the incident laser energy and absorption fraction.) An exception is that, at the time of shock reflection at the center, the broadened part of the Ar L_α emission is weaker in the second series than in the first series of experiments. This is probably because there are fewer emitters in the second series: the number of Ar ions in the targets of the second series is about half that in the first series. At the time the shock has returned halfway through the core, the predicted spectrum for the 12- μm -thick target in Fig. 45.13(b) shows absorption lines from the Li-like to the N-like states. Its lowest ionization state (N-like) is higher than that in the experimental spectrum (O-like and F-like). This implies that the absorbing outer region of the Ar core is cooler than predicted. The appearance of

Fig. 45.13

(a) Electron density (solid line) and temperature profiles (dashed line), and (b) simulated spectrum, showing the absorption lines for the 12- μm case in Fig. 45.12. The time is 515 ps with respect to the peak of the pulse. The absorption lines range from Li-like to N-like.



TC2905

absorption lines from lower ionization states than in the 6- μm case (and also in shot 15772) is caused by lower electron temperatures in the absorbing region rather than by a larger $\rho\Delta R$ in that region. This is seen in Fig. 45.13(b), which shows conditions in the Ar core: the electron temperature is about 400 to 500 eV compared to 600 to 700 eV for the 6- μm case (Fig. 45.10), while the core radii are about the same and the electron density is lower for the 12- μm case than for the 6- μm case. Both the peak electron temperature and the peak electron and ion densities are lower in the 12- μm case than in the 6- μm case: the peak electron density reached by the 12- μm -thick target is about half the density obtained by the 6- μm -thick target. The 12- μm target has a lower performance than the 6- μm target because of its larger mass and, therefore, reduced implosion velocity.

We can estimate the lower bounds of the areal density required to observe an absorption line. The optical depth of an absorption line depends on the magnitude of the integrated absorption areal ion density $n_i(r)\Delta R$ for each ionization state, where n_i is the ion density and ΔR is the incremental path length at that density. In the time-resolved spectrum for shot 15772 (Fig. 45.10), the C-like line is barely visible. In Fig. 45.11 the C-like population fraction reaches 10^{-3} over a short distance leading to an areal ion density of about $2 \times 10^{-7} n_i \text{cm}^{-2}$, or about $4 \times 10^{17} \text{cm}^{-2}$. In the second series of experiments, the N-like absorption line is slightly deeper than the C-like line in the first series. In Fig. 45.14 the population fraction for the N-like state is about 2×10^{-3} over 2 μm yielding an areal ion density of about $8 \times 10^{17} \text{cm}^{-2}$. The value of the areal ion density will vary over time as the

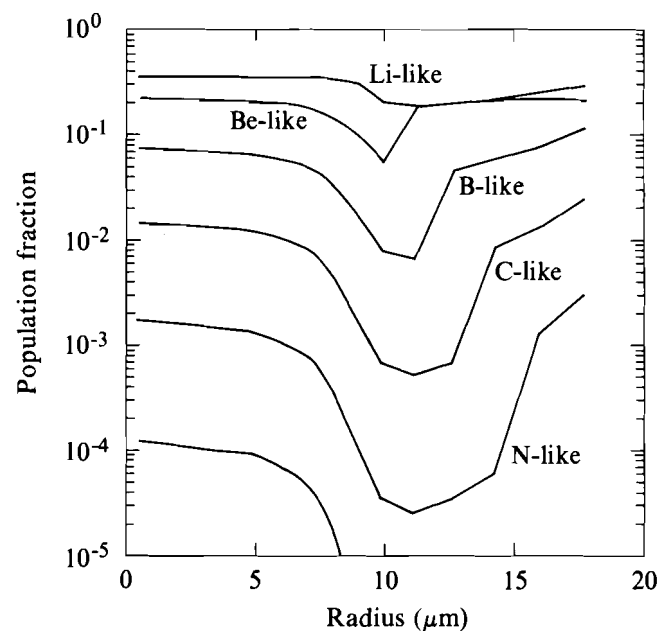


Fig. 45.14
Population fractions for the $n = 1$ to $n = 2$
inner-shell transitions for the conditions in
Fig. 45.13.

TC2903

shock travels toward the edge of the Ar core. While a quantitative analysis of the temporal variation of the areal ion density is beyond the scope of this article, we can estimate that the absorption line analysis can observe areal ion densities in Ar of about $4 \times 10^{17} \text{ cm}^{-2}$ for each ionization state. For the ionization levels computed in the simulations, this is equivalent to about $2 \times 10^{-3} \text{ g/cm}^{-2}$.

Conclusions

Two series of experiments have been analyzed in which argon-filled plastic shells were imploded to generate high-density and high-temperature conditions in the Ar core. Time-resolved and time-integrated spectra showed density-broadened emission and absorption lines. The emission lines were observed to emit about 50 ps before the absorption lines. Analysis of the emission lines from 6- μm -thick targets indicates that they originated from a plasma with electron density between $3 \times 10^{24} \text{ cm}^{-3}$ and $8 \times 10^{24} \text{ cm}^{-3}$ and temperatures ranging from 500 to 800 eV. Absorption lines from Li-, B-, and Be-like configurations were observed and their shape fitted to theoretical line shapes. The result of this analysis implies the presence of a density gradient between 1 to $2 \times 10^{24} \text{ cm}^{-3}$ and $5 \times 10^{24} \text{ cm}^{-3}$ with temperatures between 200 and 600 eV. In implosions with thicker plastic shells, the emission lines were found to be weaker and not as broadened, and absorption lines were observed for ionization states up to F-like Ar.

Simulations carried out with the 1-D hydrodynamic code *LILAC* indicate that the density-broadened lines are emitted when the shock, formed in the Ar core by the imploding CH shell, reaches the center of the target. The absorption lines are observed at a slightly later time, when the shock has reflected from the target center and is traveling back toward the shell. During this time, the central part of the Ar core emits continuum radiation caused by the high electron density ($>10^{25} \text{ cm}^{-3}$), which is absorbed in the cooler and less-dense outer region of the core. The simulations predict an electron density and temperature gradient in the absorbing region with magnitudes similar to those measured. Also, the timing of the observation of the emission and absorption spectral features agrees roughly with the code predictions. Finally, for the 12- μm -thick target, the lowest ionization state for the absorption lines is predicted to be N-like, whereas the F-like state was observed experimentally. This indicates that the electron temperature in the absorbing outer region of the core must have been lower than those predicted.

These are the first reported experiments in which the core of a target is characterized in such detail, especially after shock reflection from the center. This indicates that the target must have survived the effects of laser illumination nonuniformity and remained reasonably intact during the implosion. There are some indications, however, that the implosion was not perfectly one-dimensional: the electron temperature obtained from the analysis of the emission line is lower by a factor of 2 than the predicted temperatures, thus implying that the shock convergence was not one-dimensional. The disagreement on the lowest observable ionization state in the absorption array of the 12- μm case could be interpreted as the result of mixing of the cold

plastic-shell materials into the hotter Ar of the absorbing region. This effect was not observed in shot 15772 (6- μm shell) because the ionization state is more sensitive to small variations in electron temperature at the low ionization states than at the high ionization states.

One conclusion from the simulations is that line emission and absorption from the Ar core do not measure the peak densities attained at stagnation. Broadened emission lines can only be observed for the electron densities present at the time when the shock reaches the target center; at higher densities ($>10^{25} \text{ cm}^{-3}$) the lines merge into the continuum. The absorption lines can only furnish information about the plasma in the region between the reflected shock and the shell, whereas the peak density actually occurs behind the shock in the central part of the core. Despite these restrictions, we have shown that imploding, Ar-filled plastic targets can provide the conditions required to study the radiative properties of matter at high temperatures (about 1 keV) and high densities (about 10^{25} cm^{-3}).

ACKNOWLEDGMENT

This work was supported by the U.S. Department of Energy Division of Inertial Fusion under agreement No. DE-FC03-85DP40200 and by the Laser Fusion Feasibility Project at the Laboratory for Laser Energetics, which has the following sponsors: Empire State Electric Energy Research Corporation, New York State Energy Research and Development Authority, Ontario Hydro, and the University of Rochester.

REFERENCES

1. C. F. Hooper, Jr., D. P. Kilcrease, R. C. Mancini, L. A. Woltz, D. K. Bradley, P. A. Jaanimagi, and M. C. Richardson, *Phys. Rev. Lett.* **63**, 267 (1989).
2. R. C. Mancini, C. F. Hooper, Jr., J. Delettrez, R. Epstein, D. K. Bradley, P. A. Jaanimagi, and M. C. Richardson, in *Proceedings of the International Workshop on Radiative Properties of Hot Dense Matter*, Sarasota, FL (to be published).
3. B. L. Henke and P. A. Jaanimagi, *Rev. Sci. Instrum.* **56**, 1537 (1985).
4. L. A. Woltz and C. F. Hooper, Jr., *J. Phys. A* **21**, 4766 (1988).
5. R. C. Mancini, D. P. Kilcrease, L. A. Woltz, and C. F. Hooper, Jr., *Comp. Phys. Comm.* (to be published).
6. R. Epstein, *Phys. Fluids B* **1**, 214 (1989).
7. S. Skupsky, R. W. Short, T. Kessler, R. S. Craxton, S. Letzring, and J. M. Soures, *J. Appl. Phys.* **66**, 3456 (1989).